PAPER

Multi-channel optical router of coexisting two- and three-mode bunching

IOP Publishing Physica Scripta
Phys. Scr. 94 (2019) 085503 (6pp) https://doi.org/10.1088/1402-4896/ab1925

Multi-channel optical router of coexisting two- and three-mode bunching

Siqiang Zhang[1], Faizan Raza[1], Huanrong Fan, Yuan Feng, Al Imran, Kangkang Li and Yanpeng Zhang

Key Laboratory for Physical Electronics and Devices of the Ministry of Education, Xi'an Jiaotong University, Xi'an 710049, People's Republic of China

E-mail: ypzhang@mail.xjtu.edu.cn

Received 4 February 2019, revised 4 April 2019
Accepted for publication 15 April 2019
Published 24 May 2019

Abstract

We investigate the coexisting of two-mode and three-mode bunching in the intensity noise correlation by generating multi-order fluorescence from pseudo-thermal light source at low temperature using the Nitrogen-vacancy center in diamond. The coexisting mechanism suggests that three-mode bunching is overlapped with two-mode bunching via path indistinguishability, which can be further decomposed into multiple lower order correlation through path distinguishable offset. Moreover, the contribution from two-mode bunching in third order intensity noise correlation function is twice with respect to three-mode bunching. We demonstrate the interference among two- and three-mode bunching by controlling the time offset and dressing the slow light to realize multi-channel optical routing. Our experimental results suggest the advance technique of peak division and channel equalization ratio of about 95%, applicable to all multi-channel optical routing. The switching speed between two channels is about 20 ns.

Keywords: quantum interference, nonlinear optics, photon bunching

(Some figures may appear in colour only in the online journal)

1. Introduction

In 1956, the far-field Hanbury Brown and Twiss effect measured the second-order intensity correlation from stars which is also known as two photon bunching emerged the new insights in quantum optics [1, 2]. This Phenomena plays a vital role in the establishment and development of modern quantum theory of light [3]. Inceptively, it is also considered as a manifestation for the non-classical ghost imaging in spatial correlation [4–6]. After a while, experimental studies demonstrated for classical ghost imaging in chaotic light using nontrivial correlation of chaotic light [7–13]. Since ghost imaging with chaotic light is preferred due to adversity in generation of entangled states. Recently the photon bunching in case of polarized beam splitters has been demonstrated using Nitrogen-vacancy (NV) defects available in large density of Nano-diamond [14]. The visibility of classical second-order ghost imaging obtained by chaotic light is always low [15] as compare to obtained from correlated photon. The diamond NV center is known as photo stable defect center which is considered as an efficient chaotic light source in the fields of quantum information, quantum optics, and metrology [16].

The purpose and advantage of using NV center in diamond is that it has an individually addressable electronic spin that can be initialized and read out optically even at room temperature [17]. Tang *et al*, proposed model for NOR logical gate and a transistor switch in third order correlation resulting from nonlinear interaction among three multi-order fluorescence (MFL) signals at room temperature [18].

In this article, we present a comprehensive understanding of higher order correlation of pseudo-thermal light source in term of mode detection regime by considering single MFL as pseudo-thermal light source generated from diamond NV center. Coexistence of two- and three-mode bunching in third order intensity noise correlation is discussed. Based on experimental and simulated results, the effect of quantum path interference among two- and three-mode bunching is studied

[1] These authors contributed equally to this work.

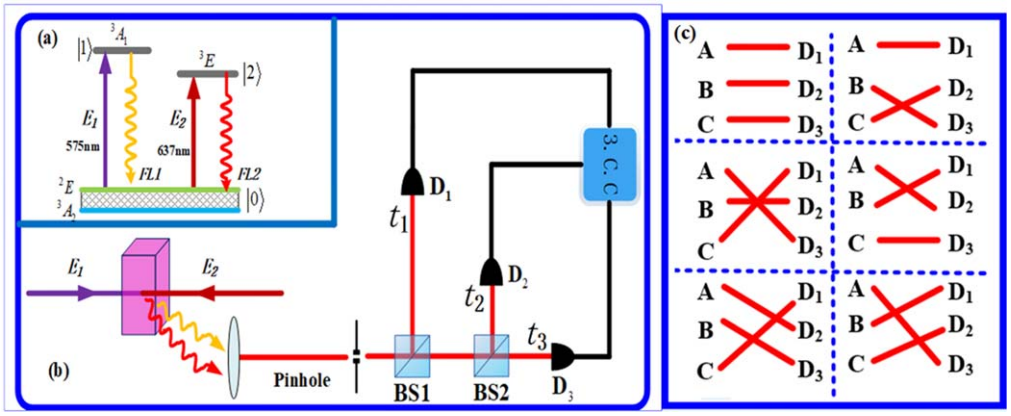

Figure 1. (a) The NV^0 and NV^- charge state inter-conversion mechanism. Excitation and fluorescence emission are designated at ZPL, which construct a V-type system. (b) shows the experimental scheme for measuring third order correlation $G^{(3)}$ for multi-order fluorescence signals emitted by a diamond NV center. (c) Three independent modes A, B and C have six alternative ways of triggering a joint detection event among detectors D_1, D_2, and D_3. At equal distances from the source, the probability of observing a three-mode joint detection event at time (t_1, t_2, t_3) is determined by the superposition of the six three-mode amplitudes.

by path distinguishable offset. Based on results, we proposed optical manipulation techniques for multi-channel routing bearing potential for the development of NV based quantum communication devices. The results are proposed for realization of such mechanism are based on the channel equalization ratio, contrast index and switching speed obtained from correlation and can be controlled by time offset and slow light effect of incident beam.

2. Basic theory

2.1. Experiment setup

The sample used in our experiment is a single diamond crystal oriented as $\langle 100\rangle$ and doped with nitrogen has concentration less than 5 part per billion. The sample was held in cryostat; the cryostat temperature was maintained at 77 K by flowing liquid nitrogen. The doped nitrogen atom creates a vacancy in diamond lattice which is treated as NV center and it exists in two charge states as NV^- and NV^0. The both charge states NV^0 and NV^- can be identified by their optical zero phonon lines at 2.156 eV (575 nm) and 1.945 eV (637 nm), respectively. The NV^0 energy levels are labelled as ^2E and $^2A_1$ for ground and excited states, respectively, while for NV^-, $^3A_2$ and ^3E represent ground and excited states, respectively. The two triplet states $^3A_2$ and ^3E are further split into three spin sublevels such as $m_s = 0$ and $m_s = \pm 1$. The energy difference between $m_s = 0$ and $m_s = \pm 1$ for triplet ground state is $D = 2.8$ GHz while for triplet excited state is $D = 1.42$ GHz, where D is also called zero field splitting. The magnetic field is applied to the sample to prevent the sub states $m_s = \pm 1$ from degeneration. The sublevels in triplet excited state is further splitted into six sub states under the combine effect of spin-spin and spin-orbital interaction due to crystal field. We can construct two and three level V-type atomic system from these sub states. Two tunable dye lasers (narrow scan with a 0.04 cm^{-1} linewidth) pumped by an injection-locked single-mode Nd:YAG laser (Continuum Powerlite DLS 9010, 10 Hz repetition rate, 5 ns pulse width) are used to generate the pumping fields $\boldsymbol{E}_1$ (575 nm), $\boldsymbol{E}_2$ (637 nm), respectively.

In this paper, we treated multi-order fluorescence generated from diamond NV center as pseudo-thermal light source. The multi-order fluorescence signal splits into three parts when it passed through two beam splitters in figure 1(b). Three signals are detected by three different detectors (D_1 D_2 and D_3), from these third order intensity noise correlation is analyzed. The contribution of second and third order intensity noise correlation for two- and three-mode bunching is investigated by changing t_i time offset ($i = 1, 2, 3\ \mu s$).

2.2. Second- and fourth-order fluorescence

The second-order fluorescence (FL) signal intensity can be described by the diagonal density matrix elements. In two-level system ($|0\rangle \leftrightarrow |1\rangle$) (see figure 1(a)), with a strong dressing field $\boldsymbol{E}_1$ (575 nm), the second-order FL process can be described by the perturbation chain $\rho_{00} \xrightarrow{\omega_1} \rho_{10}^{(1)} \xrightarrow{-\omega_1} \rho_{11}^{(2)}$, so the diagonal density matrix element is given by [19] $\rho_{11}^{(2)} = -|G_1|^2/(\Gamma_{10} + i\Delta_1 + |G_1|^2/\Gamma_{00})\Gamma_{11}$. The lifetime of FL signal can be written as $\Gamma_{FL} = \Gamma_{10} + \Gamma_{11}$ where $G_i = \mu_{ij}E_i/\hbar$ is the Rabi frequency of $\boldsymbol{E}_1$ with the electric dipole matrix elements μ_{ij} of levels $|i\rangle$ and $|j\rangle$, and Γ_{ij} is the transverse decay rate. Δ is the detuning and of pumping field $\boldsymbol{E}_1$. For the V-type level system ($|0\rangle \leftrightarrow |1\rangle \leftrightarrow |2\rangle$) (see figure 1(a)), the two tunable dye lasers are used to generate the pumping fields $\boldsymbol{E}_1$ (ω_1, Δ_1) and $\boldsymbol{E}_2$ (ω_2, Δ_2), respectively. The fourth-order fluorescence signal process can be described by the perturbation chain $\rho_{00} \xrightarrow{\omega_1} \rho_{10}^{(1)} \xrightarrow{-\omega_1} \rho_{00}^{(2)} \xrightarrow{\omega_2} \rho_{20}^{(3)} \xrightarrow{-\omega_2} \rho_{22}^{(4)}$. The transition pathways density matrix element is. $\rho_{22}^{(4)} = |G_1|^2|G_2|^2/(\Gamma_{10} + i\Delta_1)(\Gamma_{20} + i\Delta_2 + d_1^*)\Gamma_{00}\Gamma_{22}$. Where $d_1^* = |G_2|^2/[(\Gamma_{00} + |G_1|^2/(\Gamma_{20} + i\Delta_1)]$ is the nested dressing effect caused by the input fields. The lifetime of FL signal can be written as $\Gamma_{FL} = \Gamma_{10} + \Gamma_{20} + \Gamma_{00} + \Gamma_{22}$. The lifetime of the measured FL signal include coherence process between two levels $|i\rangle$ and $|j\rangle$, which can be described as decoherence rate

$\Gamma_{ij} = (\Gamma_i + \Gamma_j)/2$ $(i,\ j = 0,\ 1,\ 2,\ 3)$. Here $\Gamma_{ij} = \Gamma_{\text{pop}} + \Gamma_{\text{ion-spin}} + \Gamma_{\text{ion-ion}} + \Gamma_{\text{phonon}} + \Gamma_{\text{dressing}}$ where $\Gamma_{\text{pop}} = (2\pi T_1)_{ij}^{-1}$ (the population decay time (T_1)) depends on the location of the energy-level in phase-space, $\Gamma_{\text{ion-spin}}$ relates to the ion-spin coupling effect of the individual ion, $\Gamma_{\text{ion-ion}}$ is determined by the interaction among two charge states of NV center, and Γ_{phonon} is related to the temperature of the sample. The last three terms are components of $\Gamma_{\text{pop}} = (2\pi T_2')_{mn}^{-1}$ (the dephasing or coherence time, T_2^*). Here $(\Gamma_1)_1 = (2\pi T_1)_{11}^{-1} + (2\pi T_2^*)_{11}^{-1}$, $(\Gamma_0)_1 = (2\pi T_1)_{01}^{-1} + (2\pi T_2^*)_{01}^{-1}$ and $(\Gamma_1)_2 = (2\pi T_1)_{12}^{-1} + (2\pi T_2^*)_{12}^{-1}$. The expresses $(2\pi T_1)_{mn}^{-1}$ and $(2\pi T_2^*)_{mn}^{-1}$ in which m and n are the level-states and order number of perturbation chain, respectively. In detail, by taking the controlling terms into account, one can get $(2\pi T_1)_{11}^{-1} = (2\pi T_1)_{12}^{-1} = 8(\omega + \Delta\omega)^3\beta^2\eta^3/\varepsilon hc^3$. The term ω and $\Delta\omega$ represents the location and bandwidth of the energy-level, respectively, which can be dressed by the coupling field G_1 and G_2. Thus, the lifetime is modified since the new dressed state leads to population redistribution.

2.3. Three-mode intensity noise correlation

We have studied the third order intensity noise correlation of pseudo-thermal light source at mode detection level and phenomena of third order correlated imaging is shown in figure 1(b). The generated second- and fourth-order FL signals are treated as classical pseudo-thermal light source in a V-type system. The single FL signal is divided into three subsequent parts by two beam splitters (BS1 and BS2) adjusted as shown in figure 1(b). Three detectors (D_1, D_2 and D_3) are positioned at equal distance to monitor the mode detection at individual detector. To record the indistinguishable mode coincidence, t_1 time offset is fixed and other two times offsets (t_2 and t_3) are scanned. We discussed third order correlation based on the superposition principle in Feynman's path integral theory. The superposition principle in Feynman's path integral theory is based on the indistinguishability of different detection alternatives. The third order correlation of pseudo-thermal light comes from a coherent superposition of six different yet indistinguishable probability amplitudes, as shown in figure 1(c). There are three independent modes A, B, and C and three individual detectors D_1, D_2, and D_3. There are six different ways for the three modes to trigger the three detectors. For example, in the first case, mode A triggers detector D_1, mode B triggers detector D_2, and mode C triggers detector D_3. This is one of the ways to trigger a three-mode joint detection event. In such case the Glauber's correlation function [20] for pseudo-thermal light can be modified as

$$\begin{aligned} G^{(3)}(\tau_1, \tau_2, \tau_3) \propto 1 + \sin c^2\left[\frac{\Delta\omega(t_1 - t_2)}{2}\right] \\ + \sin c^2\left[\frac{\Delta\omega(t_2 - t_3)}{2}\right] + \sin c^2\left[\frac{\Delta\omega(t_3 - t_1)}{2}\right] \\ + 2\sin c\left[\frac{\Delta\omega(t_1 - t_2)}{2}\right] \times \sin c\left[\frac{\Delta\omega(t_2 - t_3)}{2}\right] \\ \times \sin c\left[\frac{\Delta\omega(t_3 - t_1)}{2}\right], \end{aligned} \tag{1}$$

where $\tau_1 = t_1 - t_2$, $\tau_2 = t_2 - t_3$, $\tau_3 = t_3 - t_1$, in equation (1) $\Delta\omega$ represents the bandwidth of the pseudo-thermal light source [12]. Based on phenomenon, we can name the three-mode correlation as three-mode bunching. From the quantum mechanical point of view, above mentioned bunching is the result of two- and three-mode interference, the superposition of two- and three-mode probability amplitudes. In equation (1), the first term represents the background noise, next three terms represent the two-mode bunching and last term shows three-mode bunching. The second-order correlation function can be described as

$$G^{(2)}(\tau_1) \propto 1 + \sin c^2\left[\frac{\Delta\omega(t_1 - t_2)}{2}\right]. \tag{2}$$

The correlation function defined in equation (1) is the magnitude of the interference from two- and three-mode bunching. To quantify this better, we can define the visibility as $V = (I_{\max} - I_{\min})/(I_{\max} + I_{\min})$. where $I_{\max}$ and $I_{\min}$ are the maximum and minimum of measured interference pattern, respectively. The maximum value for the visibility of the third order interference pattern with pseudo-thermal light source is measured at 71%. The reasons why the visibility cannot reach 100% in our experiments as follows. (I) The alignment of our experimental setup is not perfect. (II) The polarization of input dressing beam is not perfectly linearly polarized. In the process of fluorescence propagation, we can write susceptibility of the FL as $\varepsilon_0\chi_{\text{FL}}E_{\text{FL}} = N\mu_{11}\rho_{30}^{(1)}$ [21]. Furthermore, the group velocity of the FL signal is given as

$$v_g = \frac{c}{1 + [\omega_1(\partial\chi_{\text{FL}}/\partial\omega)\Delta_{\text{FL}=0}]/2}. \tag{3}$$

The three detectors D_1, D_2, and D_3 are placed at equal distance S to observe the mode detection at each individual detector, we can obtain dressing offset S/v_{gi} ($i = 1$, 2, and 3) when the detectors are triggered.

3. Results and discussion

Here, we analyze coexistence and interaction of two- and three-mode bunching by theoretically plotting intensity noise correlation function $G^{(3)}(\tau_1, \tau_2, \tau_3)$ from equation (1). Figure 2(a1) shows theoretical results of $G^{(2)}(\tau_1) \propto 1 + \sin c^2[\Delta\omega(t_1 - t_2)/2]$ from equation (2) for two-mode bunching measured at t_1 time offset (path distinguishable offset) $-1\,\mu$s. The peak observed in figure 2(a1) can be explained from quantum interference between two indistinguishable modes with minimum visibility measured at 33%. In view of quantum mechanical, one can predict that it is interference of two randomly distributed modes having four times higher chance of being detected at $t_1 = t_2$ than at $t_1 \neq t_2$. Figures 2(b1) and (c1) shows two-mode bunching corresponding to figure 2(a1) when t_1 time offset is 0 μs and 1 μs, respectively. Similarly, figures 2(a2)–(a3) shows simulated results for two-mode bunching plotted using equation (2). at t_2 and t_3 time offset (1 μs), respectively. Further, we also calculated the combined effect of background noise and three two-mode bunching determined by

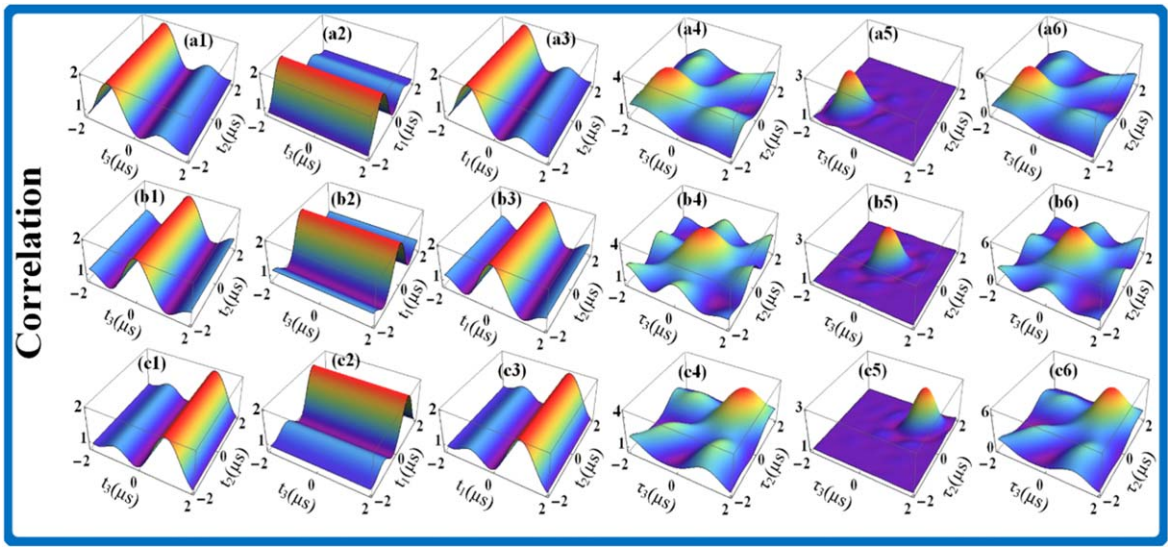

Figure 2. Illustration of coexistence of two and three-mode bunching. (a), (b) and (c) show two-mode bunching. (a4), (b4), (c4) shows combine results of two-mode bunching. (a5), (b5), (c5) shows three-mode bunching at different t_i time offset (-1, 0, 1 μs). (a6), (b6), (c6) shows coexistence of two- and three-mode bunching.

first 4 terms of equation (1) (sum of first three sinc functions) and are presented in figure 2(a4). In figure 2(a4), one center peak and three randomly distributed side peaks results from quantum interference among three two-mode bunching. Here, visibility (V) has increased up to 60%. Figures 2(b4) and (c4) shows simulated results of three two-mode bunching at t_1 time offset 0 μs and 1 μs, respectively. Subsequently, figure 2(a5) shows the theoretical results of three-mode bunching plotted by simulating the last term (product of the three sinc functions) of equation (1) whose visibility is measured at 50%. Theoretical analysis of three-mode bunching shows that it only results in one center peak and no side peaks. Figures 2(b5) and (c5) shows simulated results of three-mode bunching at t_1 time offset 0 μs and 1 μs, respectively. Finally, we investigate the coexistence of two-and three-mode bunching at different t_1 time offset -1 μs, 0 μs and 1 μs shown in figures 2(a6), (b6) and (c6), respectively. Figure 2(a6) exhibits the quantum interference among three two-mode bunching and one three-mode bunching. Furthermore, three side peaks come only from three two-mode bunching. Moreover, high correlation amplitude and greater number of peaks are observed for three two-mode bunching as compare to three-mode bunching. One can see the amplitude is increased along with visibility up to 71%. From above discussion we can conclude that two- and three-mode bunching coexist and interact with each other to increase the visibility and enhance the overall image contrast.

Figure 3 shows interaction of two- and three-mode bunching in the third order intensity noise correlation when t_1 time offset (path distinguishable offset) is changed from -1 to 1 μs. The second-order FL signal ($\rho_{11}^{(2)} = {G_1}^2/(\Gamma_{10} + \mathrm{i}\Delta_1)\Gamma_{11}$) is generated by exciting $\boldsymbol{E}_1$ (575 nm) in two-level atomic system ($|0\rangle \leftrightarrow |1\rangle$) (figure 1(a)). The single FL is divided into three beams by using two beam splitters (BS1 and BS2) and three beams are recorded at detectors (D_1, D_2, and D_3) to measure the correlation $G^{(3)}(\tau_1, \tau_2, \tau_3)$ mentioned in equation (1). Distinguishable two- and three-mode bunching at different t_1 time offset (-1, 0, 1 μs) are measured. In figure 3(a), we measured coexistence of two- and three-mode bunching by increasing t_1 time offset at fixed power (5 mW) of $\boldsymbol{E}_1$. When t_1 time offset is fixed at -1 μs, correlation curve shows one center peak and three small side peaks as shown in figure 3(a1). In figure 3(a1) center peak results from quantum interference between two- and three-mode bunching as theoretically predicted in figure 2(a) while three side peaks come from only three two-mode bunching, which corresponds to simulated in figure 2(a4). When t_1 time offset is changed to 0 μs, interference between three two-mode bunching reduces and amplitude of side peaks decreases shown in figure 3(a2) corresponding to simulated curve in figure 2(b4). At t_1 time offset 0 μs, the linewidth and amplitude of center peak also decreases owing to less interference among two- and three-mode bunching shown in figure 3(a2), which is also in well agreement with theoretical result presented in figure 2(b6). When t_i time offset is increased, location of center peak shifts and amplitude of other three peaks increases significantly due to increase in quantum interference among three-mode bunching shown in figure 3(a3). When t_i time offset is fixed at 1 μs and power of $\boldsymbol{E}_1$ is increased to 7 mW, the amplitude of side peaks increases slightly, which can be explained dressing offset (path distinguishable offset) generated by slow light effect of $\boldsymbol{E}_1$. By increasing power of $\boldsymbol{E}_1$ beam, $\rho_{11}^{(2)}$ emission along with group velocity $v_{g1} = -(\partial\rho_{10}^{(1)}/\partial\Delta_1)_{\Delta_1=0}$ and dressing offset S/v_{g1} of D_1 will change. In comparison to figures 3(a1)–(a3), figure 3(a4) shows slightly strong interference four peaks due to two offsets (1 μs and S/v_{g1}). Linewidth of correlation peaks depends upon decoherence rate Γ and bandwidth $\Delta\omega$ of pseudo-thermal light source and can be controlled by power of input beam. The splitting between dressed energy levels ($\omega + \Delta\omega$) and bandwidth ($\Delta\omega$)

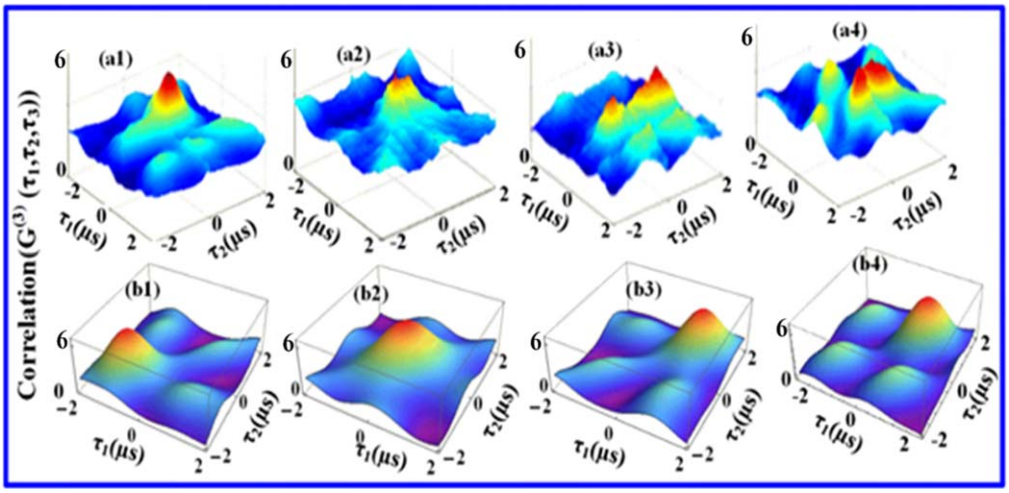

Figure 3. (a) Measured and (b) calculated the coexistence of two- and three-mode bunching by treating second-order FL as pseudo-thermal light source. (a1)–(a3) Under the condition that the power of $\boldsymbol{E}_1$ is 5 mW, the third order correlation function of the pseudo-thermal light source is measured at different t_1 time offset. (a4) The t_1 time offset is the same as that of (a3), but the power of $\boldsymbol{E}_1$ is increased by 7 mW.

increases due to strong dressing effect ($|G_1|^2/\Gamma_{00}$) at high power of $\boldsymbol{E}_1$. With increase in bandwidth ($\Delta\omega$), the correlation peaks resulting from quantum path interference become narrow as shown in figure 3(a4).

Thus, figure 3 shows interference among three two-mode bunching and one three-mode bunching. However, three two-mode bunching came out to be dominant as explained in figure 2. Figures 3(b1)–(b4) are the simulation results which replicates the same pattern of experimental data shown in figures 3(a1)–(a4). The multi-channel optical routing from coexisting two- and three-mode bunching is realized by the correlation results observed in figure 3(a). Our experiment provides a physical mechanism to realize all optical routing in the delayed time by manipulating laser power. Furthermore, we can see the division of one peak (figure 3(a2)) into four peaks (figure 3(a4)) due to change in t_1 time offset from 0 to 1 μs. Therefore, the corresponding switching ratio of our routing model is about 4. In our experiment, channel equalization ratio can be defined as $(P = 1 - \sqrt{\sum_1^{1-N}(a_i - a)^2/a})$ where a and a_i is the area of one peak and gap between the neighboring peaks, respectively, In our experiment, channel equalization ratio P increases up to 80% (figure 3(a4)) as power of input beam is increased from 5 to 7 mW. Contrast index for correlation curves can be defined as $\eta = (\tau' - \tau)/(\tau' + \tau)$, then $\eta = 80\%$ (greater accuracy of information and less crosstalk between channels), and the average power of our routing can be operated at 1–2.0 μW. The total switching speed (20 ns) is taken to be the quadrature sum of several independent contributions.

In figure 4 we investigate coexistence of two- and three-mode bunching in the third order intensity noise correlation by introducing fourth-order FL as pseudo-thermal light source. By introducing resonant beam $\boldsymbol{E}_2$ (637 nm), fourth-order FL signal is generated in three level V-type atomic system. The emitted single fourth-order FL is divided into three beams by utilizing the beam splitters (BS1 and BS2). Figures 4(a1)–(a4) shows the experimental results of indistinguishable two and three-mode quantum interference at different t_1 time offset (−1, 0, 1 μs). When t_1 time offset is changed from 0 μs (figure 4(a2)) to −1 μs(figure 4(a1)), a single broad peak is transferred of randomly distributed four peaks. This phenomenon can be attributed to increase in quantum interference among indistinguishable two-mode and three-mode bunching with the time offset. By fixing t_1 time offset at 1 μs and increasing power of $\boldsymbol{E}_1$ beam, $\rho_{22}^{(4)}$ emission along with group velocity $v_{g2} = -(\partial\rho_{20}^{(1)}/\partial\Delta_1)_{\Delta_1=0}$ and dressing offset S/v_{g2} of D_1 will change. Comparing figures 4(a1)–(a3), figure 4(a4) shows strong interference four peaks due to two offsets (1 μs and S/v_{g2}). Interference between three two-mode bunching will increase significantly due to bandwidth ($\Delta\omega$) and dressing offset generated by slow light effect resulting increase in amplitude of side peaks shown in figure 4(a4). In contrast to two-level system, bandwidth ($\Delta\omega$) of pseudo-thermal light source in a three level V-type system is low and peaks shown in figure 4(a4) are broader as compare to peaks in two-level system (figure 3(a4)). This can be explained from small splitting between dressed energy levels ($\omega + \Delta\omega$) due to nested dressing effect ($|G_2|^2/[(\Gamma_{00} + |G_1|^2/(\Gamma_{20} + i\Delta_1))$ of $\boldsymbol{E}_1$ and $\boldsymbol{E}_2$ beams. Figures 4(b1)–(b4) are theoretically calculated results of third order correlation which replicates the same behavior observed in experimental data shown in figures 4(a1)–(a4).

Thus, figures 4(a1)–(a3) shows similar interference phenomenon as described in figure 3, i-e three two- mode bunching is dominant as explained in figure 2. In figure 4(a4) shows strong four peaks interference due to equal contribution of three two-mode and one three-mode bunching. Based on two stage interference multiple peaks, one can exploit this as multi-channel optical router. In first stage of three level atomic system, one channel is converted into intermediate state four channel where channel equalization ratio (P) increases from 65% (figure 4(a2)) to 80% (figure 4(a1)) and

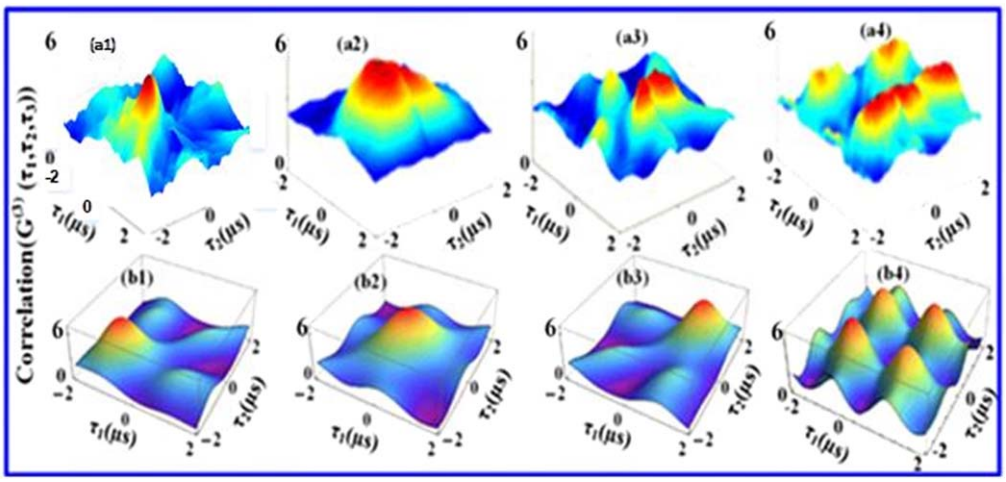

Figure 4. (a) Measured and (b) calculated the coexistence of two- and three-mode bunching. (a1)–(a3) By setting power of $\boldsymbol{E}_1$ at 5 mW, the third order correlation function of the pseudo-thermal light source is measured at different t_1 time offset. (a4) The t_1 time offset is the same as that of (a3), but the power of $\boldsymbol{E}_1$ is increased by 7 mW.

contrast index rises to $\eta = 80\%$ (figure 4(a2)) as t_1 time offset is changed from 0 to -1 μs. In second stage, when power of $\boldsymbol{E}_1$ is increased to 7 mW, intermediate state four channel are successfully converted in complete four channel and channel equalization ratio (P) increases from 80% (figure 4(a1)) to 90% (figure 4(a4)) and contrast index rises up to $\eta = 95\%$ (figure 4(a2)).

4. Conclusion

In conclusion, we investigated coexistence of two-mode and three-mode bunching in the third order intensity noise correlation by using and considering multi-order fluorescence as pseudo-thermal light source obtained from NV center in diamond. The multi-channel optical router is realized from coexistence of two and three-mode bunching in third order correlation through time offset. Channel equalization ratio, contrast index and visibility is controlled by time offset and dressing effect of input beam.

Acknowledgments

This work was supported by the National Key R&D Program of China (2017YFA0303700, 2018YFA0307500), National Natural Science Foundation of China (61605154, 11604256, 11804267).

ORCID iDs

Yanpeng Zhang https://orcid.org/0000-0002-0954-7681

References

[1] Brown R H and Twiss R Q 1956 *Nature* **177** 27–9
[2] Brown R H and Twiss R Q 1956 *Nature* **178** 1046–8
[3] Schwarzkopf A, Anderson D A, Thaicharoen N and Raithel G 2013 *Phys. Rev.* A **88** 061406
[4] Pittman T B, Shih Y H, Strekalov D V and Sergienko A V 1995 *Phys. Rev.* A **52** 3429
[5] Gatti A, Brambilla E, Bache M and Lugiato L A 2004 *Phys. Rev. Lett.* **93** 093602
[6] Strekalov D V, Sergienko A V, Klyshko D N and Shih Y H 1995 *Phys. Rev. Lett.* **74** 3600
[7] Bennink R S, Bentley S J and Boyd R W 2002 *Phys. Rev. Lett.* **89** 113601
[8] Cheng J and Han S 2004 *Phys. Rev. Lett.* **92** 093903
[9] Cai Y and Zhu S Y 2004 *Opt. Lett.* **29** 2716–8
[10] Zhang D, Zhai Y H, Wu L A and Chen X H 2005 *Opt. Lett.* **30** 2354–6
[11] Valencia A, Scarcelli G, D'Angelo M and Shih Y 2005 *Phys. Rev. Lett.* **94** 063601
[12] Ferri F, Magatti D, Gatti A, Bache M, Brambilla E and Lugiato L A 2005 *Phys. Rev. Lett.* **94** 183602
[13] Xiong J, Cao D Z, Huang F, Li H G, Sun X J and Wang K 2005 *Phys. Rev. Lett.* **94** 173601
[14] Meuret S, Tizei L H G, Cazimajou T, Bourrellier R, Chang H C, Treussart F and Kociak M 2015 *Phys. Rev. Lett.* **114** 197401
[15] Agafonov I N, Chekhova M V, Iskhakov T S and Penin A N 2008 *Phys. Rev.* A **77** 053801
[16] Maurer P C *et al* 2012 *Science* **336** 1283–6
[17] Gruber A, Dräbenstedt A, Tietz C, Fleury L, Wrachtrup J and von Borczyskowski C 1997 *Science* **276** 2012
[18] Tang H, Ahmed I, Puttapirat P, Wu T, Zhang Y and Li E 2018 *Phys. Chem. Chem. Phy.* **20** 5721–5
[19] Zheng H, Zhang X, Zhang Z, Tian Y, Chen H, Li C and Zhang Y 2013 *Sci. Rep.* **3** 1885
[20] Glauber R J 1963 *Phys. Rev.* **130** 2529
[21] Zhang Y, Brown A W and Xiao M 2006 *Phys. Rev.* A **74** 053813